

---

# Dual-Mode Deep Anomaly Detection for Medical Manufacturing: Structural Similarity and Feature Distance

Julio Zanon Diaz<sup>1</sup>, Georgios Siogkas<sup>2</sup>, and Peter Corcoran<sup>1</sup>, Fellow IEEE.

<sup>1</sup>Electrical and Electronic Engineering, University of Galway, Galway, Ireland.

<sup>2</sup>Boston Scientific, Galway, Ireland.

Corresponding author: Julio Zanon Diaz (j.zanondiaz1@UniversityofGalway.ie).

This work was supported in part by the Galway Boston Scientific's manufacturing facility.

**ABSTRACT** Automated visual inspection in medical device manufacturing faces unique challenges, including small and imbalanced datasets, high-resolution imagery, and strict regulatory requirements. To address these, we propose two attention-guided autoencoder architectures for deep anomaly detection. The first employs a structural similarity-based scoring approach that enables lightweight, real-time defect detection with unsupervised thresholding and can be further enhanced through limited supervised tuning. The second applies a feature distance-based strategy using Mahalanobis scoring on reduced latent features, designed to monitor distributional shifts and support supervisory oversight. Evaluations on a representative sterile packaging dataset confirm that both approaches outperform baselines under hardware-constrained, regulated conditions. Cross-domain testing on the MVTec-Zipper benchmark further demonstrates that the structural similarity-based method generalises effectively and achieves performance comparable to state-of-the-art methods, while the feature distance-based method is less transferable but provides complementary monitoring capabilities. These results highlight a dual-pathway inspection strategy: structural similarity for robust inline detection and feature distance for supervisory monitoring. By combining operational performance with interpretability and lifecycle monitoring, the proposed methods also align with emerging regulatory expectations for high-risk AI systems.

**INDEX TERMS** Machine Vision, Deep Anomaly Detection, Neural Networks, Advanced Manufacturing, Quality Control.

## I. INTRODUCTION

The advent of digital manufacturing, driven by Industry 4.0, is transforming traditional production processes. Automation technologies are increasingly integrated to enhance productivity, efficiency, and responsiveness to market demands. A central element of this transformation is the adoption of advanced visual-cognitive systems based on machine vision and Convolutional Neural Networks (CNNs). These systems are designed to learn complex visual features from images and make rational decisions that approach human-level cognitive capabilities.

One of the most critical applications of such technologies is automated visual inspection for defect detection. This is especially important in highly regulated sectors such as Medical Devices, where even a single missed defect (false negative) can have serious implications for patient health and safety. The regulatory environment further complicates this task, as natural defect rates are extremely low, and manufacturing processes are highly specific. These factors constrain dataset size and diversity, making the creation of large, representative defect datasets impractical within feasible timeframes.

In this work, we focus on the binary classification problem: determining whether a product is acceptable (defect-free) or defective. While segmentation approaches that provide spatial localisation of defects are valuable for root-cause analysis, regulatory priorities emphasise accurate classification. From a quality and compliance perspective, false negatives represent the most critical failure mode. For this reason, our study prioritises robust defect classification to ensure that defective parts are reliably identified and removed from production.

Despite advances in visual-cognitive technologies, the deployment of CNN-based inspection systems in manufacturing remains limited. Persistent challenges—including small datasets, imbalanced classes, and hardware constraints—reduce their suitability for industrial adoption. Consequently, many manufacturers, particularly in the Medical Device sector, continue to rely on Human Visual Inspections (HVIs). Rodriguez-Perez [1] highlights the prevalence of human error in this context, estimating that HVIs account for nearly one-third of non-conformances in medical device and pharmaceutical production.

In earlier work, we investigated the use of state-of-the-art CNNs for defect detection in sterile packaging [2]. This case was chosen as being representative of medical device inspection due to the subjectivity of defect definitions and the critical importance of avoiding false negatives. To support this research, we developed the Surface Seal Image (SSI) dataset [3], which accurately captures real-world defects encountered in medical device manufacturing. Key findings from that study included:

- Manufacturing datasets are not only small but also heavily imbalanced, with defects typically representing less than 10% of available samples.
- Images used for inspections, such as those in the SSI dataset, often exhibit low pixel complexity and limited content variation. This reduces the effectiveness of standard augmentation strategies and deep CNNs.
- State-of-the-art models performed adequately with moderately skewed datasets but degraded significantly when defect prevalence dropped to around 10%.

Building on these findings, the present work investigates methods to improve defect detection under conditions where defective samples are scarce. Specifically, we explore anomaly detection approaches that learn from defect-free data, leveraging the abundance of normal images. These methods are attractive in regulated domains, as they require minimal domain-specific optimisation and can potentially generalise across industries with specialised processes, such as medical device manufacturing.

The SSI dataset serves as the primary benchmark for our experiments. Two subsets are used: “Partial-10,” containing 10% defective samples, and “Partial-1,”

containing only 1% defective samples. These subsets enable systematic evaluation of performance under varying degrees of class imbalance. To further assess cross-domain generalisation, we extend testing to the MVTec-Zipper dataset [4], a publicly available benchmark outside the medical domain.

The contributions of this work are threefold:

1. We propose a dual-pathway architecture that combines structural similarity scoring and feature distance scoring for complementary inline and supervisory inspection.
2. We introduce attention-mask functions tailored to high-resolution, low-variability imagery, enabling efficient training on small, imbalanced datasets typical of regulated manufacturing.
3. We align the design and evaluation of our methods with emerging regulatory requirements for high-risk AI systems, ensuring both technical performance and compliance readiness.

Together, these contributions provide a foundation for anomaly detection methods that are not only effective under real-world industrial constraints but also prepared for deployment in highly regulated environments.

## II. BACKGROUND AND LITERATURE REVIEW

Convolutional Neural Networks (CNNs) achieve state-of-the-art performance when trained on large, balanced datasets with many examples per class. However, as shown in our earlier work [2] and by Yuan and Zuo [9], classification accuracy decreases sharply when training data are small or imbalanced. This limitation is particularly acute in regulated manufacturing environments, where naturally occurring defects are rare and labelled defective samples are scarce.

This section reviews existing methodologies relevant to such conditions. Section A considers approaches to improve deep learning performance with small datasets. Section B introduces anomaly detection and its relevance for regulated manufacturing. Section C focuses on deep anomaly detection methods from the literature. Section D provides a summary and key insights motivating our proposed architectures

### A. SMALL DATASETS - METHODOLOGIES TO OPTIMISE PERFORMANCE OF DEEP LEARNING MODELS

Several techniques have been developed to improve neural network performance under limited data availability: transfer learning, meta-learning, and data augmentation.

#### Transfer Learning:

Introduced by Bozinovski and Fulgosi [10], transfer learning reuses pretrained weights from one domain to accelerate training and improve performance in another. It is widely applied in vision tasks [11], reducing both training time and computational cost [12]. In medical imaging, transfer learning has improved performance in applications such as

MRI-based tumour detection [13]–[15]. However, in regulated manufacturing, defect inspection images lack the semantic richness of natural image datasets such as ImageNet. They primarily emphasise local texture irregularities. Combined with the scarcity of large labelled defect datasets, this reduces the effectiveness of transfer learning, making it insufficient for our use case.

### Meta-Learning Based Architectures

Meta-learning, or “learning to learn,” aims to generalise from very few labelled samples. Techniques such as Siamese networks [16] and Triplet-Graph Reasoning Networks (TGRN) [17] have achieved strong results in few-shot defect inspection, segmenting anomalies with as few as 1–4 labelled samples. However, our research targets conditions where hundreds of defect-free samples are available. In this scenario, meta-learning is less effective than methods that exploit the abundance of normal images.

### Dataset Augmentation

Data augmentation artificially increases dataset size by creating new image variants. Since its introduction by Krizhevsky et al. [18], augmentation has been widely applied, especially in medical imaging [19]. Yet, in manufacturing imagery such as the SSI dataset [3], low pixel complexity and limited variation often cause basic augmentation techniques to degrade performance [2], as they introduce artificial variability not present in tightly controlled inspection environments. Generative approaches, such as Defect-GAN [20], show potential but also require large training datasets, which are unavailable in our context.

### B. ANOMALY DETECTION

Anomaly detection—also known as novelty or outlier detection—identifies samples that deviate from expected norms. It has wide applications in fraud detection, medical diagnosis, and industrial fault analysis.

For image-based inspection, anomaly detection typically involves two steps:

1. Training a feature extractor on defect-free images.
2. Comparing new samples to the learned distribution of normality.

This approach is particularly attractive in regulated manufacturing because it leverages abundant defect-free data, avoids the need for extensive labelling, and reduces overfitting risks.

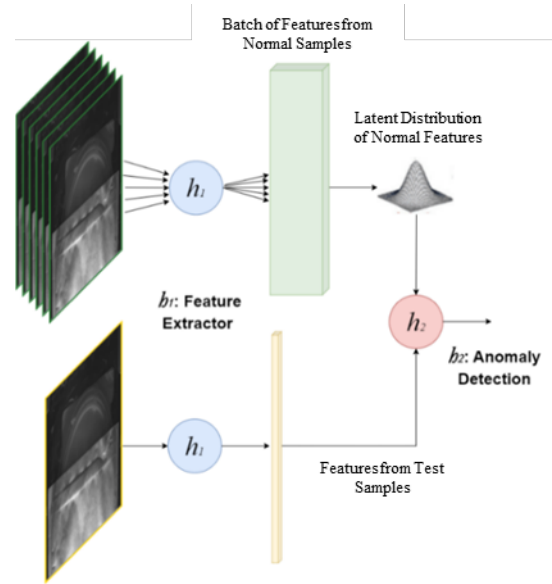


FIGURE 1. Spatial Data - Unsupervised Anomaly Detection

Early methods relied on hand-crafted feature detectors such as GFTT [21], MSER [22], and FAST [23], combined with descriptors such as BRIEF [24] or FREAK [25]. Later, SIFT [26] and SURF [27] became standard baselines by combining detection and description in a single framework. With advances in computing, CNN-based descriptors such as DeepPatch [28], LIFT [29], and R2D2 [30] surpassed these hand-crafted methods, demonstrating stronger invariance and discriminative power.

Among modern extractors, Convolutional Autoencoders (CAEs) are widely used for anomaly detection due to their ability to learn compact, non-linear representations in an end-to-end manner [31]–[33]. CAEs are effective for dimensionality reduction and denoising, making them suitable for modelling normal data distributions. Variational Autoencoders (VAEs) [34] extend CAEs by introducing probabilistic latent variables but typically require more complex tuning and offer only marginal improvements.

### C. DEEP ANOMALY DETECTION

Deep anomaly detection integrates CNNs and autoencoders into anomaly detection pipelines. A basic form is the Vanilla Autoencoder, which reconstructs normal samples and identifies anomalies via high reconstruction error [35]. Hybrid methods extend this principle by applying anomaly scoring functions directly to latent features [36].

Several advanced architectures have since been proposed:

- **MOCCA (Multilayer One-Class Classification):** Introduced by Massoli et al. [5], MOCCA combines deep autoencoders with centroid-based loss functions to compress latent feature distributions. While effective, it demands significant

computational resources, limiting its deployment in industry.

- **CPCAE (Conditional Patch-based CAE):** Saeedi and Giusti [37] adapted CAEs for high-resolution inspection by dividing images into overlapping patches with positional encoding. Although effective, it requires both normal and defective samples for training, which is often infeasible in medical device contexts.
- **RAG-PaDiM:** Kim et al. [38] extended PaDiM [39] by incorporating Attention U-Nets [40] to generate patch embeddings. These are modelled using multivariate Gaussian distributions, with anomalies detected via Mahalanobis distance. This architecture is innovative but requires labelled defective samples to initialise attention layers, exceeding the limits of small, defect-sparse datasets.

#### D. LITERATURE REVIEW SUMMARY

In summary, anomaly detection methods have advanced considerably but are often optimised for general-purpose datasets (e.g., MNIST, CIFAR-10, ImageNet) rather than manufacturing inspection. These benchmarks differ fundamentally from regulated medical device imagery, which is high-resolution, low-complexity, and constrained by both regulatory and hardware realities.

For comparison in our study, we selected four representative architectures as baselines:

- **Vanilla Autoencoder** – simple, low-complexity, usable in supervised or unsupervised modes.
- **MOCCA** – improved performance but computationally demanding.
- **CPCAE** – effective for high-resolution data but reliant on defect samples.
- **RAG-PaDiM** – innovative embeddings but dependent on supervised initialisation.

These limitations underscore the need for approaches specifically designed for medical device inspection, where datasets are small, defects are scarce, and compliance requirements are stringent.

### III. PROPOSED ARCHITECTURE and METHODS:

We propose two architectures that achieve comparable performance and can be trained either in **unsupervised mode**, using only defect-free samples, or in **supervised mode**, where a small number of defective samples are used to optimise threshold selection. Both designs are inspired by recent deep anomaly detection models but are tailored to the specific characteristics of medical device manufacturing imagery.

These images are typically high-resolution, and aggressive down-sampling often degrades performance. At the same time, hardware limitations in manufacturing environments constrain the maximum image size that can be processed

efficiently. To address this, our methods adopt a **hybrid patch-based strategy** similar to RAG-PaDiM and CPCAE.

#### A. Attention-Mask Strategy and Autoencoder Backbone

Performance is further enhanced by exploiting the highly structured nature of medical device imagery. Image acquisition systems are engineered to minimise variability in factors such as part positioning, tilt, and magnification. Although defective samples are scarce, their properties are generally well characterised through risk assessments and controlled experiments. This knowledge allows accurate localisation of regions where defects are most likely to occur. In the case of the SSI dataset, subject matter experts confirmed that the defect class under investigation appears exclusively along the seal region.

To take advantage of this, we introduce **attention masks** that define **variable regions of interest (ROIs)**. Unlike fixed patching across the entire image, attention masks dynamically select ROI coordinates by applying a sequence of steps:

1. **Edge-preserving smoothing** using bilateral filtering [43].
2. **Gradient-based edge detection**, such as the Canny operator [44].
3. **Histogram profile analysis** along vertical and horizontal directions to refine the optimal ROI.

For the SSI dataset, this process detects pouch material transition edges and then fixes ROI size (i.e., patch), supported by the stability of the acquisition system. In general, this approach can be extended to generate multiple ROIs per image through an array of patch functions. However, because all SSI defects are contained within a single region, only one patch function was required.

Formally, each mask function outputs coordinates  $(x_0, y_0)$ ,  $(x_1, y_1)$  for patch  $i$  of image  $j$ :

$$F_i(\text{Image}_j) = \text{Attention} - \text{Patch}_{ij} \quad \text{Equation 1}$$

Both of our proposed methods build on this shared backbone: a **Convolutional Autoencoder (CAE) with four latent layers**, trained to reconstruct each attention patch using only defect-free samples. Reconstruction loss is measured using **mean squared error (MSE)**.

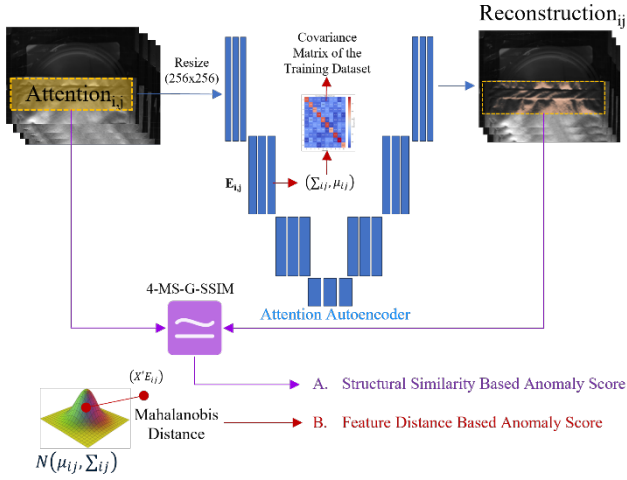


**FIGURE 2. Attention Autoencoder with Anomaly Detection Score methods**

FIGURE 2 illustrates the shared architecture. The backbone attention autoencoder is common to both methods, while the anomaly detection stage branches into two scoring approaches: structural similarity (Method B) and feature distance (Method C).

### B. Structural Similarity Based Anomaly Score

In the first approach, once the autoencoder has been trained, anomaly scores are computed by comparing the **structural similarity** between original and reconstructed patches. For this, we adopt an extended version of the **Structural Similarity Index (SSIM)** introduced by Wang et al. [45].

Unlike pixel-wise metrics such as MSE or PSNR, SSIM evaluates similarity by combining luminance, contrast, and structural information. Formally, SSIM for two image patches  $x$  and  $y$  is given as:

$$SSIM(x, y) = \frac{(2\mu_x\mu_y + C_1)(2\sigma_{xy} + C_2)}{(\mu_x^2 + \mu_y^2 + C_1)(\sigma_x^2 + \sigma_y^2 + C_2)} \quad \text{Equation 2}$$

Where  $\mu_x, \mu_y$  are the local means of  $x$  and  $y$ ,  $\mu_x^2, \mu_y^2$ , their variances,  $\sigma_{xy}$  the covariance and  $C_1, C_2$  are the constants to stabilise the division.

Renieblas et al. [47] later extended SSIM for radiological image analysis, proposing variants such as **4-MS-G-SSIM**. This extension integrates four components: luminance similarity, contrast similarity, structural similarity, and gradient similarity, while assessing similarity at multiple resolutions. This multi-scale design increases sensitivity to structural distortions, making it well suited for anomaly detection.

Once anomaly scores  $\mathcal{L}_{ij}$  are obtained for each patch “ $i$ ” of each image “ $j$ ” in the training dataset, an **unsupervised anomaly threshold** can be determined using only defect-free samples:

$$T_{Unsupervised} = \mu_{normal} + 2\sigma_{normal} \quad \text{Equation 3}$$

where

$$\mu_{normal} = \frac{1}{N_0} \sum_{i=1}^{N_0} \mathcal{L}_i \quad \text{Equation 4}$$

and

$$\sigma_{normal} = \sqrt{\frac{1}{N_0 - 1} \sum_{i=1}^{N_0} (\mathcal{L}_i - \mu_{normal})^2} \quad \text{Equation 5}$$

With  $\{\mathcal{L}_i\}_{i=1}^{N_0}$  denoting the anomaly scores of the  $N_0$  defect-free samples.

This threshold encompasses  $\sim 97.7\%$  of the normal distribution, with higher values flagged as potential defects.

Alternative thresholding strategies were also evaluated:

- **Extreme Value Theory (EVT):** Discarded due to insufficient normal samples for stable tail fitting.
- **Empirical 95th percentile:** Comparable to  $\mu + 2\sigma$  but less interpretable.

Ultimately, the  **$\mu + 2\sigma$  rule** (Equation 3) was selected for its statistical clarity and suitability for regulated environments.

In supervised settings, thresholds can instead be optimised by maximising classification accuracy on the training set:

$$T_{Supervised} = \underset{T \in [0,1]}{\operatorname{argmax}} \frac{1}{N} \sum_{i=1}^N 1((\mathcal{L}_i \geq T) \Leftrightarrow (y_i = 1)) \quad \text{Equation 6}$$

where  $N$  is the number of training samples, and  $y_i \in \{0,1\}$  indicates its ground-truth class label (0 = defect-free, 1 = defective). This formulation explicitly leverages both classes to identify the threshold that maximises classification performance on the training data.

### C. Feature Distance Based Anomaly Score

The second method operates directly on latent features, inspired by MOCCA and RAG-PaDiM. Rather than reconstructing images, it computes anomaly scores from **embeddings extracted at layer 2** of the autoencoder.

Specifically, the **Mahalanobis distance** is calculated between the embeddings  $E_{ij}$  from layer 2 of the autoencoder and the corresponding multivariate Gaussian distribution  $N(\mu_{ij}, \Sigma_{ij})$  learned during training:

$$M(x_{ij}) = \sqrt{(E_{ij} - \mu_{ij})^T \Sigma_{ij}^{-1} (E_{ij} - \mu_{ij})} \quad \text{Equation 7}$$

To reduce computational overhead in hardware-constrained environments, we randomly select 500 features from layer 2. This balances efficiency and detection performance.

Thresholds for this method can also be defined in either unsupervised mode (Equation 3) or supervised mode (Equation 6).

#### D. Summary

In summary, both methods share a common **attention-based autoencoder backbone** (FIGURE 2) but diverge in how anomaly scores are computed:

- **Structural similarity** compares reconstructed patches against their originals, providing perceptual anomaly scoring.
- **Feature distance** measures deviations in latent feature distributions, enabling lightweight storage and distributional monitoring.

Together, these approaches provide complementary capabilities, optimised for the unique demands of defect detection in medical device manufacturing.

## IV. EXPERIMENTAL METHODOLOGY

The objective of the experiments is to evaluate the performance of the proposed architectures against both a simple deep anomaly detection baseline—the Vanilla Autoencoder—and more advanced models, including MOCCA, CPCAe, and RAG-PaDiM. Beyond benchmarking, the experiments also aim to empirically validate key design choices underlying our architectures. All evaluations were carried out under realistic manufacturing conditions, using restricted training hardware, comparable optimisation procedures, and datasets with only a small number of defective samples, which are particularly suited to supervised approaches.

Reproducibility presented practical challenges. For CPCAe and RAG-PaDiM, no public code was available, so implementations were recreated based on the descriptions provided in the original publications. In the case of MOCCA, the original architecture could only be executed on CPU with restrictions on training quantity and image size due to its high memory requirements. To enable fair comparison, we therefore evaluated both the original CPU implementation and a customised version adapted to run on GPU hardware.

#### A. Hardware Configuration and Code Repository

The hardware used for the experiments reflects typical industry-level setups employed in the development of manufacturing applications. Although no detailed study was carried out to quantify the impact of hardware limitations on training performance, constraints on computing capacity were introduced deliberately. The primary objective of this research is to design deep anomaly detection solutions that can be

deployed within common manufacturing environments, and based on our experience, we consider the selected hardware representative of such conditions. These environments often operate with limited resources, as manufacturing applications are typically bespoke and do not generally justify substantial investment in high-end infrastructure.

All experiments were conducted on a workstation with the following configuration:

- CPU: Intel Core™ i7.
- GPU 1: RTX4080, 16GB, 640 Tensor Cores, 9728 CUDA Cores.
- RAM: 64GB DDR4, 2400MHz.
- Hard Drive: SSD 1TB, 7,000 MB/s.

#### B. Image Data Set

Experiments were conducted using the publicly available Surface Seal Image (SSI) Dataset of Sterile Barrier Packaging [3], which contains two classes: normal samples and defective samples. This dataset reflects typical manufacturing conditions in terms of image quality and composition and provides multiple subsets with varying degrees of class imbalance, ranging from 1% to 50% defective samples.

The primary objective of our proposed architecture is to achieve optimal performance in the unsupervised setting, that is, when trained exclusively with defect-free samples. However, our methodology also accommodates the use of a limited number of defective samples for anomaly threshold selection, reflecting the practical reality of medical device datasets, where only a small proportion of defective samples are typically available. The SSI dataset therefore offers an appropriate basis for experimentation under both conditions.

As highlighted by our previous research [2], in collaboration with industry partners, defect rates in highly regulated manufacturing industries are typically as low as 0.1%. Given typical production volumes, assembling ~1,000 samples with a 50% defect rate could require up to 2.5 years of production, making such datasets impractical. To simulate realistic industrial conditions, we adopted two training and cross-validation subset ‘Partial-10’, containing 10% defective samples, used during the development and testing of the architecture; and ‘Partial-1’, containing 1% defective samples, used to challenge experimentation.

In addition to these training and cross-validation subsets, a balanced dataset (‘Test-split’) was used exclusively for final testing. This subset was not involved in architectural design decisions, ensuring maximum generalisation potential and objective evaluation. Table 1 summarises the dataset configurations employed in our experiments.

Table 1. SSI Dataset Sub-Sets

Sub-Set Name	Description	Image quantities		
		Total	Good	Defects
'Partial-10'	Training and Cross-Validation	424	382	42
'Partial-1'	Training and Cross-Validation	424	420	4
'Test-split'	Testing	360	180	180

It is important to note that while the selected subsets enable the evaluation of supervised approaches, they impose limitations on unsupervised methods. Based on typical manufacturing volumes [2], a six-month data collection period could yield more than 50,000 normal samples, which would be expected to significantly improve the performance of unsupervised models trained solely on defect-free data. At present, however, no publicly available datasets of this scale meet the requirements of our research. Although this limitation does not preclude meaningful experimentation, future studies should consider repeating these evaluations with larger normal-only datasets.

FIGURE 3 illustrates a representative image from the 'Partial-10' training and cross-validation subset.

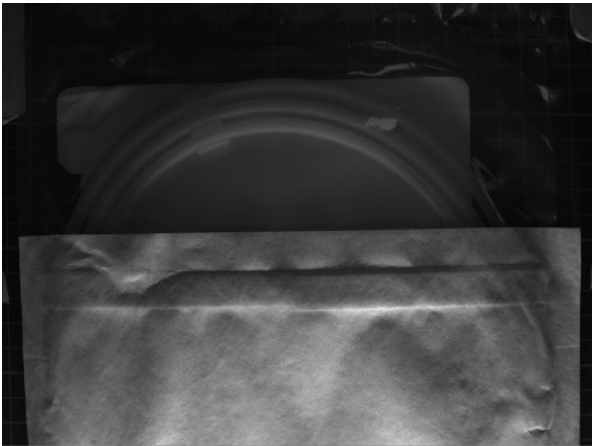


FIGURE 3. SSI dataset example

To evaluate the validity of the proposed methods on external datasets, we repeated the final experiments using the "Zipper" class of the MVTec dataset and compared our results with publicly available benchmarks. This class was selected because its images are monochrome, high resolution, and exhibit defects similar to those commonly encountered in the medical device industry, which is the focus of this research. FIGURE 3 illustrates an example image from this dataset.

The MVTec-Zipper dataset contains 240 defect-free samples for training, and 32 defect-free samples together with 119 defective samples for testing. As the test set is highly imbalanced, and to enable comparison with the publicly available results reported in [5], we employ the Balanced Accuracy (BA) defined by the following equation:

$$BA = \frac{TP}{2 \cdot (TP + FN)} + \frac{TN}{2 \cdot (TN + FP)} \quad \text{Equation 8}$$

### C. Model Implementation and Optimisation approach

**Scripting:** Code is available in repository <https://github.com/JulioZanon/Structural-Similarity-and-Feature-Distance-Based-Deep-Anomaly-Detection-for-High-Resolution-Images>.

**Image Pre-processing:** No preprocessing of images is carried out other than resizing images to 256x256 to overcome hardware performance constraints.

### Optimisation approach:

Hyperparameter tuning techniques included Bayesian optimiser and grid searches. Due to hardware limitations, batch sizes were limited to low values. To produce consistent benchmarking indicators, we omitted the use of k-folds and instead randomly split the training set into Training and Xval splits (80% / 20%) with a fix seed.

## V. EXPERIMENTAL RESULTS

The first set of experiments, trained with the 'Partial-10' subset, was designed to establish a baseline for developing our methodology. For this purpose, we implemented and trained both basic and advanced deep anomaly detection architectures from the literature, including the Vanilla Autoencoder as well as more recent models such as MOCCA, CPCAe, and RAG-PaDiM. These experiments also introduced the use of attention-patch functions within the autoencoder framework.

It is important to note that, with the exception of MOCCA and PaDiM, the original source code for these architectures was not publicly available. Our implementations therefore followed the published architectural descriptions as closely as possible. Nonetheless, incomplete implementation details and differences in preprocessing or training procedures make exact reproduction unlikely. Consequently, the results presented for CPCAe, AG-PaDiM, and RAG-PaDiM should be regarded as reference benchmarks rather than strict replications of the original models published by the authors. This highlights both the reproducibility challenges in anomaly detection research and the importance of open-source availability for fair and transparent evaluation.

Table 2. Benchmark Study Trained with SSI “partial-10” and results obtained from the SSI Test subset

Model	AUC	ACC	P	R	F1
<sup>a</sup> MOCCA Original	0.676	0.634	0.679	0.528	0.594
<sup>b</sup> MOCCA GPU Adaptation	0.724	0.694	0.639	0.894	0.745
<sup>b</sup> CPCAE	0.817	0.742	0.664	<b>0.978</b>	<b>0.791</b>
Padim	0.720	0.664	0.620	<b>0.844</b>	0.716
<sup>b</sup> AG-Padim	0.664	0.598	1.000	0.748	0.664
<sup>b</sup> RAG-Padim	0.500	0.500	1.000	0.667	0.500
Vanilla AE (4 Layers)	0.614	0.614	<b>0.936</b>	0.244	0.388
<sup>b</sup> AAE-MSE	<b>0.881</b>	<b>0.708</b>	0.931	0.450	0.607

**a:** Trained with a reduce quantity of samples and downsized images to overcome memory limitations (240 samples with size 1024x1024)

**b:** Custom adaptation of state-of-the-art architecture.

From these results, we inferred that the Vanilla Autoencoder, when enhanced with attention-patch functions (Referred to as AAE), demonstrated strong potential for performance improvement. However, recall remained very low, indicating that the autoencoder with MSE anomaly score was biased toward the normal class on which it was trained. In the context of quality inspections in highly regulated industries, this finding is critical, as missed defect detections can have serious implications, underscoring the need for methods that preserve recall while maintaining robustness in highly regulated inspection environments.

The optimisation of the vanilla autoencoder to determine a 4-layers architecture was carried out by setting a 2-steps optimisation script with a Bayesian optimiser and the hyperparameters in Table 12 and Table 13 in Appendix B.

It is also important to note that the MOCCA feature extraction approach is highly memory intensive. The architecture uses an autoencoder with selection blocks in all encoder layers to progressively reduce the feature space through convolutional operations. These features are mapped into hyperspheres whose volumes are gradually reduced during training. In addition, the original implementation applied extensive data augmentation within the training function, which required loading the entire dataset into memory during training. As a result of these design choices, the original code could not be executed on the SSI dataset using the full 382 samples at their native resolution. The reported results in Table 2 were therefore obtained only after scaling their size to match the MVTec-Zipper dataset (1024x1024 pixels). In our GPU adaptation, we mitigated some of these memory constraints by removing augmentation—considered domain-specific and more appropriately treated as a preprocessing step—to enable fairer

performance comparisons between models. We also used custom gradient checkpointing to allow efficient calculation of the selectors and reduced the batch size from 128 in the CPU version to 8 to allow training in GPU, a change that likely impacted performance. Furthermore, our implementation used selectors from all layers by default, in contrast to the original default setup that used only the one from the latent space. Future work should repeat experiment related to the original MOCCA implementation with hardware capable of supporting larger batch sizes and native image resolution. Nonetheless, the focus of our research is on developing architectures and methodologies deployable at scale in manufacturing environments, and we believe the hardware limitations imposed here accurately reflect the constraints of typical industrial training pipelines.

### a) Structural Similarity-Based Scoring

In the second set of experiments, we evaluated different variants of the SSIM index family for anomaly scoring in our first proposed approach. These included metrics originally proposed by Li and Bovik [46] and later extended by Renieblas et al. [47]. All models were trained on the “Partial-10” subset, with anomaly thresholds determined in supervised mode.

Table 3. Attention AE Anomaly Detection with Supervised Threshold and results obtained from the SSI Test subset

Model	AUC	ACC	P	R	F1
MSE	0.881	0.708	0.931	0.450	0.607
SSIM	0.930	0.825	0.838	0.806	0.822
PSNR	0.866	0.744	0.855	0.589	0.697
MAE	0.915	0.781	0.885	0.644	0.746
MS-SSIM	0.922	0.808	0.840	0.761	0.799
4-SSIM	0.969	0.867	0.817	<b>0.944</b>	0.876
4-MS-SSIM	<b>0.977</b>	<b>0.931</b>	<b>0.938</b>	0.922	<b>0.930</b>
4-G-SSIM	0.530	0.500	0.500	0.028	0.053
4-MS-G-SSIM	0.843	0.700	0.853	0.483	0.617

Among these, 4-MS-SSIM achieved the best overall balance of sensitivity and robustness, corroborating the findings reported in [46].

It is noteworthy that the gradient-extended variant (4-G-SSIM) degraded markedly, with accuracy dropping to 0.530. The ‘G’ denotes the inclusion of a gradient similarity term, which measures consistency of local edge information between the input and reconstruction. While this component enhances sensitivity to structural distortions, in our experiments it proved overly sensitive to small reconstruction artefacts in defect-free samples, leading to a high false positive rate. By contrast, the multi-scale variants (4-MS-SSIM and 4-MS-G-SSIM) stabilised this sensitivity by averaging across resolutions, yielding robust improvements. This highlights the

importance of multi-scale integration when incorporating gradient-based similarity

As an additional experiment, we investigated whether performance could be improved by replacing the single-score thresholding strategy with a supervised machine learning model that integrates multiple descriptors. Specifically, we aggregated anomaly scores from the SSIM variants and combined them with Gray Level Co-occurrence Matrix (GLCM)-based texture features, originally proposed by Haralick et al. [48], which capture second-order statistical dependencies of pixel intensities. These feature vectors were then used to train Random Forest (RF), Support Vector Machine (SVM), and Logistic Regression (LR) classifiers to optimise decision boundaries.

Table 4. ML Threshold Selection from model trained in SSI and metrics reported in Table 3.

Model	ACC	P	R	F1
RF	0.914	<b>0.916</b>	<b>0.911</b>	<b>0.914</b>
SVM	0.900	0.891	<b>0.911</b>	0.901
LR	<b>0.956</b>	0.717	0.819	0.842

Although the supervised models achieved competitive results, only logistic regression (ACC 0.956) marginally outperformed the simpler supervised thresholding of 4-MS-SSIM (ACC 0.931). This indicates that, while the approach may provide some benefit in borderline cases, the added complexity of integrating heterogeneous descriptors offers limited practical value for this dataset.

Finally, we compared unsupervised thresholding of the 4-MS-SSIM method with supervised thresholding trained on two subsets: the ‘‘Partial-10’’ split, containing 42 defective samples (10% of the dataset), and the ‘‘Partial-1’’ split, containing only 4 defective samples (1% of the dataset).

Table 5. 4-MS-SSIM - Supervised vs Unsupervised Threshold and results obtained from the SSI Test subset

Model	ACC	P	R	F1
Supervised (Trained Partial-10)	<b>0.931</b>	0.938	0.922	<b>0.930</b>
Supervised (Trained Partial-1)	0.803	<b>0.991</b>	0.611	0.756
Unsupervised	0.903	0.847	<b>0.983</b>	0.910

As expected, supervised thresholding—when trained with an abundant number of defective samples (10% or above)—delivered slightly higher accuracy and precision. However, the gain was marginal, reinforcing the viability of our architecture in a fully unsupervised setting, which is particularly advantageous in domains where defective samples are scarce. More importantly, while recall was poor when the supervised model was trained with only 1% defective samples, recall remained high for the other two configurations (0.922 for

supervised with 10% and 0.983 for unsupervised). This demonstrates that both approaches can be reliably deployed for defect inspection in highly regulated manufacturing processes.

### b) Feature-Distance-Based Scoring

The third set of experiments focused on the second proposed method, evaluating strategies for extracting latent features and computing anomaly scores. Again, the ‘Partial-10’ subset was used, with thresholds set in supervised mode and results reported on the Training subset to avoid overfitting.

Given hardware limitations, several dimensionality reduction methods were tested, including Principal Component Analysis (PCA) with a variable retention of components to capture 95% of variation, Independent Component Analysis (ICA), and random feature drop (initially reducing to 500 features). Two approaches were then evaluated for anomaly scoring: K-Means clustering and Mahalanobis distance.

Table 6. All Features in Covariance Matrix trained on and reported from SSI ‘‘Partial-10’’ subset

Model	AUC	ACC	P	R	F1
PCA-K-Means	0.663	0.617	0.566	0.994	0.722
PCA-M	0.543	0.500	0.500	1.000	0.667
K-Means	0.446	0.519	0.516	0.633	0.569
ICA-M	0.463	0.492	0.200	0.006	0.011
Random Drop – K-Means	0.589	0.589	0.554	0.906	0.688
Random Drop – M	<b>0.909</b>	<b>0.836</b>	<b>0.789</b>	<b>0.917</b>	<b>0.848</b>

From this analysis, we concluded that random feature drop combined with Mahalanobis distance provided the most effective balance of computational efficiency and detection accuracy.

We justify random feature reduction through an intuition related to the Johnson–Lindenstrauss lemma: high-dimensional embeddings can be projected into much lower dimensions while approximately preserving pairwise distances. Although our reduction is based on random feature selection rather than dense random projections, the same principle applies: provided the reduced dimension remains sufficiently large, anomaly-relevant distances are preserved with high probability. This perspective helps explain why our method maintains discriminative power despite aggressive dimensionality reduction

It is worth noting that by aggressively reducing feature dimensionality, we alleviate the need for shrinkage-based covariance regularisation, as the reduced covariance matrices are well-conditioned and can be reliably estimated with the available normal samples

### c) Feature Extraction Ablation Study

An ablation study was then conducted to determine the optimal degree of feature reduction using random drop, and to evaluate whether features extracted from specific autoencoder layers outperform those extracted from all layers. This study was again carried out using only the images in the training dataset to avoid overfitting. Results are provided in Appendix A – Table 10 and Table 11, showing that a random feature selection of 500 to 1000 features, from Layer 1 or layer 2, performed similarly, achieving the best trade-off between computational efficiency and performance with 500 randomly selected features from layer 2.

To confirm these findings, we repeated the experiments using features from Layers 1 and 2, applying random drop, with training on the ‘Partial-10’ subset and thresholds set in unsupervised mode. These results are again obtained on the training dataset to avoid overfitting.

Table 7. Mahalanobis distance trained on and reported from SSI “Partial-10” subset

Model	AUC	ACC	P	R	F1
RandomDrop-Layer1	0.910	0.850	<b>0.812</b>	0.911	0.859
RandomDrop-Layer2	<b>0.920</b>	<b>0.861</b>	0.801	<b>0.961</b>	<b>0.874</b>

This confirmed that features in both individual layers, 1 and 2, offer similar anomaly detection capabilities, achieving an accuracy of 0.850 and 0.861 respectively against training data, and outperforming any of the methods in Table 6, using all layers, as report.

Finally, we compared supervised versus unsupervised thresholding for random drop in layer 2, using the Test subset.

Table 8. RandomDrop-Layer2 Supervised vs Unsupervised Threshold trained on SSI “Partial-10” subset and reported from Test subset

Model	ACC	P	R	F1
Supervised	<b>0.722</b>	<b>0.643</b>	<b>1.000</b>	<b>0.783</b>
Unsupervised	0.658	0.594	<b>1.000</b>	0.745

As expected, supervised thresholding achieved higher accuracy, though still significantly lower than the performance observed on the Training subset. To better understand this gap, we examined histogram in FIGURE 4, which depicts the distribution of Mahalanobis distances for both the Training and Test subset.

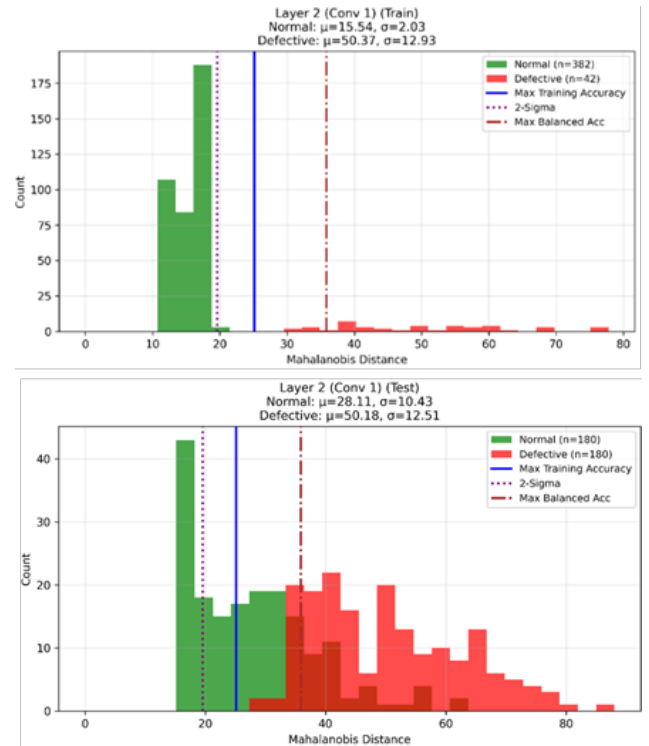


FIGURE 4. Histogram of Mahalanobis distances for Training (top) and Test (bottom) datasets

As observed, the distributions of defective samples were highly consistent across datasets, with nearly identical means (50.37 in Training vs. 50.18 in Test) and similar standard deviations (12.93 vs. 12.51). In contrast, the distributions of normal samples diverged markedly: the Training dataset exhibited a narrow spread (standard deviation = 2.03), whereas the Test dataset showed a much broader spread (standard deviation = 10.43).

These findings suggest that the backbone autoencoder strongly overfitted to the training data. This was intentional by design: the model was developed to overfit on the normal class, which is typically abundant, so that it generalises poorly on defective samples and produces higher anomaly scores. In practice, this approach requires a very large pool of normal images to ensure that the learned representation captures the true variability of the defect-free class. In our experiments, however, the number of normal samples in training (382) was modest compared to the number in the Test set (180), leading to higher variance in unseen normal images. This mismatch reduced precision by causing false positives. We therefore expect that with much larger quantities of defect-free samples—more representative of the real distribution—the model would better approximate the normal class and yield the intended effect of discriminating defects without penalising unseen but valid normal samples.

As a result of the relatively low number of testing samples, distinguishing anomalous from normal features became more

difficult, lowering generalisation performance and, in particular, precision. In practical terms, this would translate into an inspection system prone to generating high levels of false scrap.

On the other hand, the method’s sensitivity to variations in image composition could be leveraged in supervisory contexts. While less suitable for automated online edge inspection, it may provide significant value in post-production analysis, where shifts in feature distributions could be monitored to detect or even predict emerging manufacturing issues.

#### d) Generalisation with external datasets

We further evaluated the two proposed methods on the MVTec-Zipper dataset, applying only minimal optimisation to assess their ability to generalise. Results were compared with those reported for MOCCA using Maximum Balanced Accuracy (MaxBA) and with the metrics published by the MVTec authors. It should be noted that the MVTec classification results were presented only as per-class accuracy, from which Balanced Accuracy was derived.

Table 9. MVTec-Zipper dataset results comparing our proposed approach with MOCCA results

Model	AUC	MaxBA
Our method with anomaly score based on <b>4-MS-SSIM</b> (all images)	0.747	0.742
Our method with anomaly score based on <b>4-MS-SSIM</b> (removing 31 defects in fabric)	0.801	<b>0.806</b>
Our method with anomaly score based on <b>Mahalanobis distances</b> (all Images)	0.552	0.55
<sup>a</sup> MOCCA	0.84	0.78
<sup>b</sup> MVTec AE <sub>SSIM</sub>	---	0.7
<sup>b</sup> MVTec AE <sub>L2</sub>	---	0.689
<sup>b</sup> MVTec AutoGan	---	0.566
<sup>b</sup> MVTec CNN Feature Dictionary	---	0.531

**a:** Results reported in [5]; **b:** Results reported in [4].

As shown in Table 9, our structural similarity-based approach did not reach the higher accuracy achieved on the SSI dataset, yet its performance remained comparable to MOCCA, albeit slightly lower and superior to all other methods reported by MVTec. The feature distance-based method, however, failed to achieve meaningful performance and was deemed unsuitable for this dataset. To investigate this disparity observed in the structural similarity-based approach, we analysed the Zipper images and observed two distinct classes of defects located in different regions: defects in the zipper itself and defects in the surrounding fabric (FIGURE 5). Because our method relies on well-defined defect regions to generate attention masks, this characteristic explains the

reduced performance. To test this intuition, we repeated the experiment excluding the less represented class (defects in the fabric, with 31 of the 119 defective samples). As reported in Table 9, the 4-MS-SSIM method then improved markedly, with MaxBA increasing from 0.742 to 0.806, confirming our hypothesis.

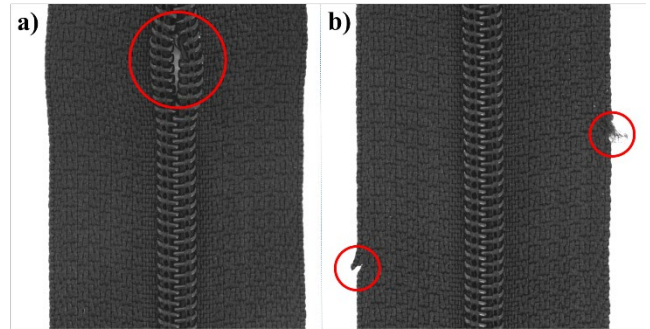


FIGURE 5. MVTec Zipper dataset defect examples with red circles highlighting the defects. a) defects in the Zipper, b) defects in the fabric.

These findings confirm that, although the feature distance-based method does not generalise well to external datasets from other domains, the structural similarity-based approach remains competitive with state-of-the-art methods. They also highlight that our attention-mask strategy is inherently constrained in its ability to support cross-domain generalisation, pointing to a clear avenue for future research and development aimed at achieving broader applicability.

It is important to acknowledge that these results are limited by the use of only one external dataset. While demonstrating generalisation on datasets outside the medical device domain is valuable, the scope of this research is intentionally focused on medical device inspections. At present, no publicly available datasets exist in this field. Consequently, although broader validation is desirable, extensive testing on unrelated industrial datasets would not directly advance the goals of this work. Instead, the priority lies in generating and validating representative medical device datasets, which we identify as a key avenue for future research.

## VI. DISCUSSIONS

Our baseline evaluation showed that while MOCCA, CPCAE, PaDiM, AG-PaDiM, and RAG-PaDiM are recent and innovative, their re-implementations on the SSI dataset did not achieve competitive results. In many cases, performance was comparable to that of a simple Vanilla Autoencoder. Because source code for CPCAE, AG-PaDiM and RAG-PaDiM was not publicly available, we relied on textual descriptions, which may have introduced discrepancies in preprocessing, hyperparameters, or training schedules. For this reason, we report them as **reference benchmarks** rather

than exact replications. This highlights ongoing reproducibility challenges in anomaly detection research.

#### a) *Impact of Attention-Mask Functions*

The introduction of attention masks substantially improved performance. Vanilla AE accuracy increased from 0.614 to 0.708 once attention patches were applied. Although designed specifically for the SSI dataset, attention masks are likely generalisable to other medical device inspection tasks, where parts are consistently positioned and defects occur in predictable regions. Future extensions could include full-image attention overlays with adaptive loss weighting, enabling the detection of anomalies beyond predefined ROIs.

#### b) *Structural Similarity–Based Method*

The structural similarity–based method (4-MS-SSIM) achieved strong results on the SSI dataset:

- **Unsupervised thresholding:** 0.903 accuracy
- **Supervised thresholding with 10% defects:** 0.931 accuracy
- **Supervised thresholding with 1% defects:** 0.803 accuracy, recall 0.611

These results indicate that supervised tuning is only beneficial when sufficient defective samples are available. With very few defective samples, supervised training risks unacceptable defect escape rates in regulated manufacturing. Importantly, all configurations surpassed benchmark baselines, demonstrating the robustness of this approach even in unsupervised mode.

Experiments where SSIM was used directly as a training loss confirmed this degraded separability of anomalies. This supports the use of **MSE for reconstruction** and **SSIM for post hoc anomaly scoring** as complementary roles.

#### c) *Feature Distance–Based Method*

The feature distance–based method, inspired by MOCCA and RAG-PaDiM, was redesigned for hardware-constrained environments by reducing  $\sim 1,000,000$  latent features to 500 randomly selected features from Layer 2. Results showed:

- **Supervised mode:** 0.722 accuracy
- **Unsupervised mode:** 0.658 accuracy
- **Recall:** 1.0 in both cases, but with low precision (high false scrap)

Analysis of Mahalanobis-score distributions revealed strong overfitting to the normal class (i.e. defect-free samples). This behaviour was intentional, as the model is designed to overfit defect-free samples so that anomalies (i.e. defective samples) receive higher scores. In practice, however, very large pools of normal images would be required to capture the true variability of defect-free products. With the modest training size available, unseen normal samples exhibited high variance, leading to reduced precision.

Despite this limitation for inline inspection, the method’s sensitivity to changes in the normal class is valuable for **supervisory monitoring**. In post-production settings,

tracking feature distributions over time can reveal process drift or emerging manufacturing issues. This aligns with emerging requirements for lifecycle monitoring under the EU AI Act.

#### d) *Generalisation to External Datasets*

When tested on the MVTEC-Zipper dataset, the methods showed contrasting performance:

- **Structural similarity–based method:** MaxBA 0.742 (all classes) and 0.806 (restricted to zipper defects only), close to or exceeding the best reported baseline (MOCCA, 0.780).
- **Feature distance–based method:** MaxBA 0.55, unsuitable for this dataset.

The lower performance on the full Zipper dataset compared with SSI can be explained by two factors:

1. **Higher complexity:** The Zipper dataset includes more varied textures, making a shallow autoencoder insufficient.
2. **Multiple defect classes:** Defects occur both in the zipper and surrounding textile, while our method assumes well-defined defect regions. This reduced the effectiveness of the attention-mask strategy.

These results confirm that while the feature distance–based method does not generalise well across domains, the structural similarity–based approach remains competitive with state-of-the-art methods. At the same time, they highlight that cross-domain performance is limited, and that the methods are best suited to structured medical device imagery, where defect regions are predictable.

#### e) *Complementary Deployment Strategy*

Taken together, our findings indicate that the two proposed methods are complementary:

- **Structural similarity–based method:** Best suited for real-time, inline inspection, where high recall and efficiency are essential.
- **Feature distance–based method:** Better suited for supervisory or cloud-based monitoring, where compact latent features can be stored, analysed over time, and compared against golden reference distributions.

Because both methods share the same attention-based autoencoder backbone, they can be deployed in tandem: one for robust defect detection at the edge, the other for long-term monitoring of process drift.

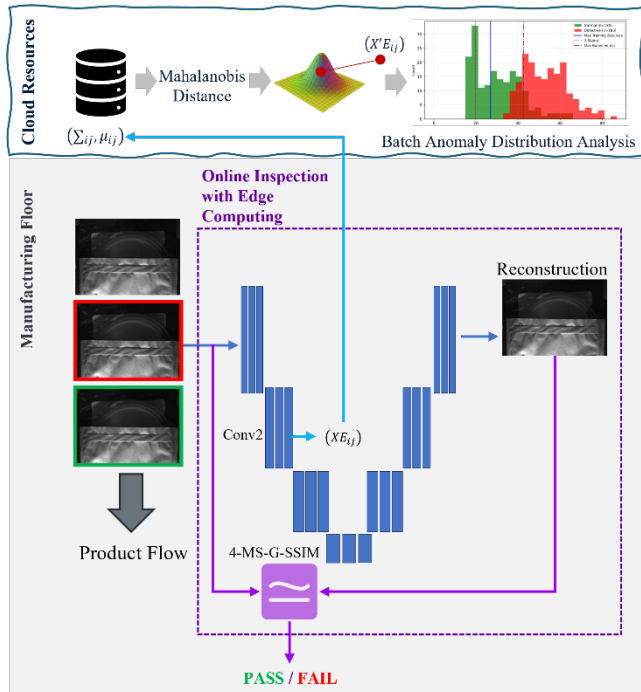


FIGURE 6. Practical deployment framework for the proposed anomaly detection methods.

#### f) Regulatory Alignment

The alignment of our methods with regulatory expectations is significant. Under the **EU AI Act** [50], AI systems used in Class III medical device manufacturing are classified as high-risk and must demonstrate risk management, explainability, and post-deployment monitoring. Similarly, the **FDA draft guidance** [49] highlights the importance of transparency and lifecycle surveillance.

Our dual approach maps naturally to these obligations:

- **Interpretability:** The SSIM-based method provides explainability through transparent similarity scores and visual overlays of reconstruction error.
- **Monitoring:** The feature distance-based method enables distributional monitoring of latent features, ensuring lifecycle governance and supporting traceability of past results.

Together, these methods offer both operational performance and regulatory readiness, providing a practical foundation for AI deployment in safety-critical manufacturing environments.

## VII. CONCLUSIONS AND FUTURE WORK

In this work, we proposed and evaluated two attention-guided autoencoder architectures for deep anomaly detection in medical device manufacturing. Both methods address the challenges of small, imbalanced datasets and hardware constraints, offering practical solutions for regulated environments.

- **Structural similarity-based anomaly scoring:** Using the 4-MS-SSIM index, this method achieved 0.903 accuracy in unsupervised mode and 0.931 with supervised tuning using 10% defective samples. Its robustness and efficiency make it well suited for inline, edge-based deployment on production lines.
- **Feature distance-based anomaly scoring:** Using Mahalanobis distance on 500 randomly reduced features from Layer 2, this method achieved 0.722 accuracy (supervised) and 0.658 (unsupervised). Although limited by low precision, its sensitivity to distributional change makes it valuable for supervisory monitoring and lifecycle governance.

Both supervised and unsupervised thresholding strategies were tested. While supervised tuning provided marginal gains with sufficient defective samples, unsupervised thresholding remained highly competitive and more suitable for generalisation. Across all configurations, our methods consistently outperformed baselines (MOCCA, CPCAE, PaDiM, AG-PaDiM, RAG-PaDiM) under hardware-constrained conditions, reinforcing the importance of open and reproducible benchmarks.

### External Validation

To assess generalisation, both methods were evaluated on the MVTEC-Zipper dataset. The structural similarity-based method achieved performance comparable to state-of-the-art (MaxBA 0.742 for all defect types, 0.806 when restricted to zipper defects). The feature distance-based method, however, was unsuitable for this dataset. These results confirm competitiveness with existing methods but also highlight that cross-domain generalisation remains limited.

### Future Work

Several directions are planned to extend this research:

1. **Full-image attention overlays** with weighted loss functions, enabling detection of defects outside predefined ROIs and improving adaptability across domains.
2. **Hybrid training objectives** that combine MSE and SSIM to benefit from both pixel-level fidelity and perceptual sensitivity.
3. **Principled feature reduction strategies** such as attention-based ranking or sparsity constraints, replacing random feature selection while retaining discriminative features.
4. **Validation on larger medical device datasets** containing predominantly normal samples (i.e. defect-free samples), enabling the intentional overfitting strategy to better capture variability of defect-free products.
5. **Expansion of benchmarking datasets** through the creation and dissemination of domain-specific repositories, as no public datasets currently exist for medical device inspection.

6. **Development of regulatory alignment protocols**, including model release dossiers and qualification strategies tailored to the requirements of the EU AI Act.
7. **Replication of MOCCA** and other high-resource models on more powerful hardware, enabling training on the full SSI dataset (382 images at native resolution). This will allow for a more balanced evaluation of performance and memory trade-offs.

### Concluding Remarks

Beyond technical contributions, the proposed methods provide practical mechanisms for interpretability and monitoring. Reconstructed images allow pixel-level error maps to be visualised alongside global similarity scores, supporting traceability and human oversight. In parallel, latent feature storage enables long-term monitoring against golden references, with the flexibility to refine models as additional production data become available.

In conclusion, the proposed architectures combine inline defect detection with supervisory monitoring, offering a dual-purpose inspection strategy that addresses both operational requirements and regulatory standards. Results on the MVTec-Zipper dataset confirm competitiveness with state-of-the-art approaches, while also reinforcing that the greatest potential of these methods lies in structured medical device inspection scenarios. The relative performance of MOCCA, however, must be interpreted with caution: its implementation in this study was constrained by hardware limitations, and improved results are likely with more capable resources. Our comparative advantage should therefore be viewed in the context of practical deployment constraints typical of manufacturing environments. By emphasising interpretability, robustness in small-data regimes, and lifecycle monitoring, this work anticipates emerging compliance obligations under the EU AI Act [50] and forthcoming FDA guidance [49], strengthening its relevance for deployment in safety-critical and highly regulated environments.

## REFERENCES

- [1] J. Rodríguez-Pérez, "Human Error Reduction in Manufacturing", 2023, American Society for Quality, Quality Press, Milwaukee 53203, ISBN: 978-1-63694-090-8
- [2] J. Zanon Diaz, M.A. Farooq, P. Corcoran, "Automatic inspection of seal integrity in sterile barrier packaging: a deep learning approach", 2024, IEEE Access, 22904–22927, DOI:10.1109/ACCESS.2023.3348779.
- [3] J. Zanon Diaz, P. Corcoran, "Surface seal image dataset of sterile barrier packaging", 2024, Science Direct - Data in Brief, Vol. 57, 2352-3409, DOI:10.1016/j.dib.2024.110996.
- [4] P. Bergmann, M. Fauser, D. Sattlegger and C. Steger. "MVTec AD — A Comprehensive Real-World Dataset for Unsupervised Anomaly Detection"; in: IEEE/CVF Conference on Computer Vision and Pattern Recognition (CVPR), 9584-9592, 2019, DOI:10.1109/CVPR.2019.00982.
- [5] F.V. Massoli, F. Falchi, A.Kantarci, S. Akti, H.K. Ekenel, and G. Amato, "MOCCA: Multilayer One-Class Classification for Anomaly Detection". 2022, IEEE Transaction on Neural Networks and Learning Systems, vol. 33, no. 6, 2022, pp. 2313–2323. DOI:10.1109/TNNLS.2021.3130074.
- [6] T. Daniel, T. Kurutach, and A. Tamar, "Deep Variational Semi-Supervised Novelty Detection", 2019, DOI:10.48550/arXiv.1911.04971.
- [7] I. Kim, Y. Jeon, J.W. Kang and J. Gwak, "RAG-PaDiM: Residual Attention Guided PaDiM for Defects Segmentation in Railway Tracks", 2023, Journal of Electrical Engineering & Technology, no. 18(2), pp. 1429–1438. DOI:10.1007/s42835-022-01346-2.
- [8] J. Saeedi, and A. Giusti, A., "Semi-supervised visual anomaly detection based on convolutional and transfer learning", 2023, Machine Learning with Applications, no.11, pp.100451. DOI:10.1016/j.mlwa.2023.100451.
- [9] Q. Yuan and Z. Zuo, "Research on the Performance of different Convolutional Neural Network Models on small Datasets," 2022, International Conference on Machine Learning and Intelligent Systems Engineering (MLISE), Guangzhou, , pp. 57-62, DOI:10.1109/MLISE57402.2022.00019.
- [10] S. Bozinovski and A. Fulgosi, "The influence of pattern similarity and transfer learning upon training of a base perceptron B2" (original in Croatian), 1976, Proceedings of Symposium Informatica 3-121-5.
- [11] K. Weiss, T.M. Khoshgoftaar and D. Wang, "A survey of transfer learning", 2016, Journal of Big Data 3, 9.
- [12] DS. Terzi, "Effect of Different Weight Initialization Strategies on Transfer Learning for Plant Disease Detection.", 2024, Plant Pathology, vol. 73, no. 9, pp. 2325–2343, DOI:10.1111/ppa.13997.
- [13] N. Tajbakhsh, J. Y. Shin, S. R. Gurudu, R. T. Hurst, C. B. Kendall, M. B. Gotway, and J. Liang, "Convolutional neural networks for medical image analysis: Full training or fine tuning?" IEEE Trans. Med. Imag., vol. 35, no. 5, pp. 1299–1312, May 2016, DOI:10.1109/TMI.2016.2535302.
- [14] D. R. Clymer, J. Long, C. Latona, S. Akhavan, P. LeDuc, and J. Cagan, "Applying machine learning methods toward classification based on small datasets: Application to shoulder labral tears," J. Eng. Sci. Med. Diag. Therapy, vol. 3, no. 1, p. 1, Feb. 2020, DOI:10.1115/1.4044645.
- [15] N. Arunkumar, M. A. Mohammed, S. A. Mostafa, D. A. Ibrahim, J. J. P. C. Rodrigues, and V. H. C. de Albuquerque, "Fully automatic model-based segmentation and classification approach for MRI brain tumor using artificial neural networks", 2022, Concurrency Comput., Pract. Exper., vol. 32, no. 1, pp. e496, DOI:10.1002/cpe.4962.
- [16] A. Shaban, S. Bansal, Z. Liu, I. Essa, and B. Boots, "One-shot learning for semantic segmentation," 2017, DOI:10.1709.03410.
- [17] Y. Bao, K. Song, J. Liu, Y. Wang, Y. Yan, H. Yu, and X. Li, "Triplet-graph reasoning network for few-shot metal generic surface defect segmentation", 2021, IEEE Trans. Instrum. Meas., vol. 70, no. 5011111, DOI:10.1109/TIM.2021.3083561.
- [18] A. Krizhevsky, I. Sutskever, and G. E. Hinton, "ImageNet classification with deep convolutional neural networks", 2017, Commun. ACM, vol. 60, no. 6, pp. 84–90, DOI: 10.1145/3065386.
- [19] Z. Eaton-Rosen, F. Bragman, S. Ourselin, and M. J. Cardoso, "Improving data augmentation for medical image segmentation", 2018, in Proc. 1st Conf. Med. Imag. Deep Learn.
- [20] G. Zhang, K. Cui, T.-Y. Hung, and S. Lu, "Defect-GAN: Highfidelity defect synthesis for automated defect inspection", 2021, in Proc. IEEE Winter Conf. Appl. Comput. Vis. (WACV), pp. 2524–2534.
- [21] J. Shi, "Good features to track", In 1994 Proceedings of IEEE conference on computer vision and pattern recognition, pp. 593-600. DOI:10.1109/CVPR.1994.323794.
- [22] J. Matas, O. Chum, M. Urban, and T. Pajdla, "Robust wide-baseline stereo from maximally stable extremal regions". 2004, Image and vision computing, Vol.22(10), pp.761-767, DOI:10.1016/j.imavis.2004.02.006.
- [23] E. Rosten, and T. Drummond, "Machine learning for high-speed corner detection". 2006, In Computer Vision–ECCV 2006: 9th European Conference on Computer Vision, Part I 9, pp. 430-443. DOI:10.1007/11744023\_34.
- [24] M. Calonder, V. Lepetit, C. Strecha, and P. Fua, "Brief: Binary robust independent elementary features". 2010, In Computer Vision–ECCV 2010: 11th European Conference on Computer Vision, Proceedings, Part IV 11, pp. 778-792. DOI:10.1007/978-3-642-15561-1\_56.
- [25] A. Alahi, R. Ortiz, and P. Vandergheynst, "Freak: Fast retina keypoint". 2012, In 2012 IEEE conference on computer vision and pattern recognition, pp. 510-517. DOI:10.1109/CVPR.2012.6247715.
- [26] D.G. Lowe. "Object recognition from local scale-invariant features". 1999, In Proceedings of the seventh IEEE international conference on computer vision, Vol. 2, pp. 1150-1157. DOI:10.1109/ICCV.1999.790410.
- [27] H. Bay, T. Tuytelaars, and L. Van Gool, L. "SURF: Speeded up robust features". 2006, In Computer Vision–ECCV 2006: 9th European Conference on Computer Vision, Proceedings, Part I 9, pp. 404-417. DOI:10.1007/11744023\_32.
- [28] E. Simo-Serra, E. Trulls, L. Ferraz, I. Kokkinos, P. Fua, and F. Moreno-Noguer. "Discriminative learning of deep convolutional feature point descriptors". 2015, In Proceedings of the IEEE international conference on computer vision, pp. 118-126. DOI:10.1109/ICCV.2015.22.
- [29] K.M Yi, E. Trulls, V. Lepetit, and P. Fua. "Lift: Learned invariant feature transform". 2016, In Computer Vision–ECCV 2016: 14th European Conference, Proceedings, Part VI 14, pp. 467-483. DOI:10.1007/978-3-319-46466-4\_28.
- [30] J. Revaud, C. De Souza, M. Humenberger, and P. Weinzaepfel. "R2d2: Reliable and repeatable detector and descriptor". 2019, Advances in neural information processing systems, Vol.32. DOI:10.48550/arXiv.1906.06195.
- [31] H. Bourlard, and Y. Kamp. "Auto-association by multilayer perceptrons and singular value decomposition". 1988, Biological cybernetics, Vol. 59(4), pp.291-294. DOI:10.1007/bf00332918.
- [32] J. Masci, U. Meier, D. Ciresan, and J. Schmidhuber. "Stacked convolutional auto-encoders for hierarchical feature extraction". 2011, In Artificial Neural Networks and Machine Learning–ICANN 2011: 21st International Conference on Artificial Neural Networks, Espoo, Proceedings, Part I 21, pp. 52-59. DOI:10.1007/978-3-642-21735-7\_7.
- [33] M. Usman, S. Latif, and J. Qadir. "Using deep neural networks for facial expression recognition". 2017, In 2017 13th International Conference on Emerging Technologies (ICET), pp. 1-6. DOI:10.1109/ICET.2017.8281753.
- [34] N. Žizakić, and A. Pižurica. "Efficient local image descriptors learned with autoencoders". IEEE Access, Vol. 10, pp.221-235. DOI:10.1109/ACCESS.2021.3138168.
- [35] R. Changala, P.K. Yadav, M. Farooq, M.S. Al Ansari, V.A. Vuyyuru, and S. Muthuperumal. "Advancing Surveillance Systems: Leveraging Sparse Auto Encoder for Enhanced Anomaly Detection in Image Data Security". 2024, In 2024 International Conference on Data Science and Network Security (ICDNSNS), pp.1-6. DOI:10.1109/ICDNSNS62112.2024.10691001.
- [36] S. Kumari, and C. Prabha. "A Comprehensive Review of Deep Anomaly Detection Techniques-An Analysis". 2024, In 2024 IEEE 9th International Conference for Convergence in Technology (I2CT), pp. 1-6. DOI:10.1109/I2CT61223.2024.10543335.

- [37] J. Saedi, and A. Giusti. "Semi-supervised visual anomaly detection based on convolutional autoencoder and transfer learning". 2023, *Machine Learning with Applications*, Vol.11, pp.100451. DOI:10.1016/j.mlwa.2023.100451.
- [38] I. Kim, Y. Jeon, J.W. Kang, and J. Gwak. "RAG-PaDiM: residual attention guided PaDiM for defects segmentation in railway tracks". 2023, *Journal of Electrical Engineering & Technology*, Vol.18(2), pp.1429-1438. DOI:10.1007/s42835-022-01346-2.
- [39] T. Defard, A. Setkov, A. Loesch, and R. Audigier. "Padim: a patch distribution modeling framework for anomaly detection and localization". 2021, In *International Conference on Pattern Recognition*, pp. 475-489. DOI:10.1007/978-3-030-68799-1\_35.
- [40] O. Oktay, J. Schlemper, L.L. Folgoc, M. Lee, M. Heinrich, K. Misawa, K. Mori, S. McDonagh, N.Y. Hammerla, B. Kainz and B. Glocker. "Attention u-net: Learning where to look for the pancreas", 2018, arXiv preprint DOI:10.48550/arXiv.1804.03999.
- [41] N. Otsu, "A Threshold Selection Method from Gray-Level Histograms," in *IEEE Transactions on Systems, Man, and Cybernetics*, vol. 9, no. 1, pp. 62-66, Jan. 1979,. DOI: 10.1109/TSMC.1979.4310076.
- [42] P.C. Mahalanobis, "On the generalised distance in statistics". 1936, *Proceedings of the National Institute of Sciences of India*, 2(1), 49–55.
- [43] C. Tomasi, and R. Manduchi, "Bilateral filtering for gray and color images". 1998, *Sixth International Conference on Computer Vision*. Bombay, pp. 839–846. DOI:10.1109/ICCV.1998.710815.
- [44] J. Canny, "A computational approach to edge detection". 1986, *IEEE Transactions on pattern analysis and machine intelligence*, (6), pp.679–69.
- [45] Z. Wang, A. C. Bovik, H. R. Sheikh, and E. P. Simoncelli, "Image quality assessment: from error visibility to structural similarity," *IEEE Transactions on Image Processing*, vol. 13, no. 4, pp. 600–612, Apr. 2004.
- [46] C. Li and A. C. Bovik, "Content-partitioned structural similarity index for image quality assessment," *Signal Processing: Image Communication*, vol. 25, no. 7, pp. 517–526, Aug. 2010, DOI:10.1016/j.image.2010.03.004.
- [47] G. P. Renieblas, A. T. Nogués, A. M. González, N. Gómez-León, and E. G. del Castillo, "Structural similarity index family for image quality assessment in radiological images," *Journal of Medical Imaging*, vol. 4, no. 3, p. 035501, July 2017. DOI:10.1117/1.JMI.4.3.035501.
- [48] Haralick, R. M., Shanmugam, K., & Dinstein, I. (1973). Textural features for image classification. *IEEE Transactions on Systems, Man, and Cybernetics*, SMC-3(6), 610–621. DOI:10.1109/TSMC.1973.4309314.
- [49] U.S. Food and Drug Administration, *Considerations for the Use of Artificial Intelligence to Support Regulatory Decision-Making for Drug and Biological Products: Guidance for Industry and Other Interested Parties, Draft Guidance*, Jan. 2025. [Online]. Available: <https://www.fda.gov/regulatory-information/search-fda-guidance-documents/considerations-use-artificial-intelligence-support-regulatory-decision-making-drug-and-biological>.
- [50] European Parliament and Council of the European Union, "Regulation (EU) 2024/1684 of the European Parliament and of the Council of 12 July 2024 laying down harmonised rules on artificial intelligence (Artificial Intelligence Act)," *Official Journal of the European Union*, L 164, Aug. 2024.



**Julio Zanon Diaz** received his degree in Telecommunications Engineering from the University of Valencia, Spain, in 2000, prior to the Bologna Process reforms that aligned third-level degrees across Europe. He later returned to the University of Valencia to complete a B.Eng. (Hons.) in Electronics in 2017. Since 2001, he has worked as an automation engineer in the automotive and medical device industries, gaining

recognised expertise in equipment design, safety, software development, robotics, and machine vision. He is currently a Fellow Engineer at Boston Scientific, where he leads strategies and teams in the development and deployment of advanced manufacturing technologies, with a focus on data science, artificial intelligence, digital twins, and human-centric manufacturing. Mr. Zanon Diaz is also pursuing a Ph.D. in Electrical and Electronic Engineering at the University of Galway, Ireland. His research interests include automated visual inspection using computer vision and deep neural networks in highly regulated manufacturing environments. He previously served as a part-time Adjunct Lecturer with the University of Galway.



**George Siogkas** (Member, IEEE) is a Senior R&D Consultant and the founder of Irish company CVRLab, specializing in Computer Vision and Machine Learning. He has worked as a R&D Computer Vision engineer for leading companies in the fields of Autonomous Driving and Medical Devices and is currently working with Boston Scientific. He holds a Ph.D. in Electrical and Computer Engineering from the University of Patras,

Greece, as well as an MSc and MEng in related fields. Throughout his career, he has combined academic roles with industry positions focused on applied research and development in Computer Vision and Pattern Recognition, and has contributed to advancing methods in Computer Vision both through research published in peer-reviewed international journals and conferences and through cutting-edge research for product development, including projects at various stages from concept to commercialization.



**Peter Corcoran** (Fellow, IEEE) currently holds the Personal Chair of Electronic Engineering with the College of Science and Engineering, University of Galway. He was the Co-Founder of several start-up companies, notably FotoNation (currently the Imaging Division, Xperi Corporation). He has more than 600 cited technical publications and patents, more than 120 peer-reviewed journal articles, 160

international conference papers, and a co-inventor on more than 300 granted U.S. patents. He is an IEEE fellow recognized for his contributions to digital camera technologies, notably in-camera red-eye correction and facial detection. He is also a member of the IEEE Consumer Technology Society for more than 25 years and the Founding Editor of IEEE Consumer Electronics Magazine.

## Appendix A. Random Feature Selection – Ablation Study

Table 10. Feature Random Selection Ablation Study – Accuracy, trained on and reported from SSI “Partial-10” subset

Layer	100	200	500	600	1000	1500
Run 1-Conv_1	0.525	0.522	0.850	0.856	0.853	0.847
Run 1-Conv_2	0.497	0.497	0.861	0.861	0.869	0.831
Run 1-Conv_3	0.506	0.533	0.797	0.797	0.792	0.817
Run 1-Bottleneck	0.500	0.500	0.500	0.500	0.500	0.494
Run 2-Conv_1	0.503	0.775	0.842	0.864	0.867	---
Run 2-Conv_2	0.519	0.519	0.850	0.811	0.819	---
Run 2-Conv_3	0.511	0.517	0.811	0.797	0.797	---
Run 2-Bottleneck	0.500	0.500	0.500	0.500	0.500	---
Run 3-Conv_1	0.514	0.511	0.861	0.875	0.844	---
Run 3-Conv_2	0.514	0.511	0.831	0.864	0.847	---
Run 3-Conv_3	0.514	0.519	0.803	0.789	0.803	---
Run 3-Bottleneck	0.500	0.500	0.500	0.500	0.500	---
Avg-Conv_1	0.514	0.603	<b>0.851</b>	<b>0.865</b>	<b>0.855</b>	---
Avg-Conv_2	0.510	0.509	<b>0.847</b>	<b>0.845</b>	<b>0.845</b>	---
Avg-Conv_3	0.510	0.523	0.804	0.794	0.797	---
Avg-Bottleneck	0.500	0.500	0.500	0.500	0.500	---

Table 11. Random Selection Ablation Study – Time to Test

Layer	100	200	500	600	1000
Conv_1	19.4 ms	34.6 ms	49.6 ms	52.3 ms	134.2 ms
Conv_2	19.1 ms	30.6 ms	<b>48.2 ms</b>	51.9 ms	131.9 ms
Conv_3	17.6 ms	30.2 ms	44.8 ms	50.1 ms	131.2 ms
Bottleneck	11.5 ms	14.3 ms	12.4 ms	12.2	12.0 ms

## Appendix B. Optimisation of Backbone Autoencoder

Table 12. Autoencoder Architecture Optimisation – Step 1 (Bold denotes best performing parameters locked for next step)

Parameter Name	Fix parameter or Search Range
Encoder filters per layer and number of layers	[(32, 64, 96), (32, 64, 128), <b>(32, 64, 96, 128)</b> , <b>(16, 32, 64, 128)</b> , (16, 32, 96, 128, 160), (16, 32, 96, 128, 160, 192), (32, 64, 128, 256), (32, 64, 128, 256, 512)]
Learning Rate	0.00001 to 0.01
Number of Epochs	20 to <b>100</b>
Optimiser Function	[ <b>Adam</b> , SGD, RMSProp]
Loss function	[mse, mae, ssim]
Dropout rate	(0.0, 0.5) (uniform) [ <b>0.11228</b> ]

Table 13. Autoencoder Architecture Optimisation – Step 2 (Bold denotes best performing parameters selected for the final autoencoder)

Parameter Name	Fix parameter or Search Range
Encoder filters	[(16, 32, 64, 128), <b>(32, 64, 128, 256)</b> ] (categorical indices)
Batch size	[16, <b>32</b> , 64, 128] (categorical)
Learning Rate	<b>0.001</b> to 0.01 (uniform)
Optimiser Function	<b>Adam</b> (fixed)
Optimiser Parameters	$\beta_1$ : ( <b>0.90</b> to 0.99) (uniform) $\beta_2$ : ( <b>0.9990</b> to 0.9999) (uniform) epsilon: ( $1e^{-8}$ to $1e^{-5}$ ) (uniform) [ <b><math>1e^{-7}</math></b> ]
Loss function	[ <b>mse</b> , mae, ssim] (categorical)
Dropout rate	<b>0.11228</b> (fixed)

## Appendix C. Thresholding ablation study

Table 14. Attention AE Anomaly Detection Thresholding Accuracy  $\mu+2\sigma$  vs 95<sup>th</sup> Percentile

Model	ACC ( $\mu+2\sigma$ )	ACC (95 <sup>th</sup> Percentile)
MSE	0.742	<b>0.767</b>
SSIM	<b>0.875</b>	0.864
PSNR	0.739	<b>0.767</b>
MAE	0.817	<b>0.833</b>
MS-SSIM	<b>0.869</b>	0.858
4-SSIM	<b>0.864</b>	0.850
4-MS-SSIM	<b>0.903</b>	0.886
4-G-SSIM	<b>0.500</b>	0.483
4-MS-G-SSIM	0.553	<b>0.767</b>